Study of microstructure in $SrTiO_3$/Si by high-resolution transmission electron microscopy

G.Y. Yang
Materials Research Science and Engineering Center, University of Maryland, College Park, Maryland 20742

J.M. Finder and J. Wang
Physical Science Research Laboratories, Motorola Inc., Tempe, Arizona 85284

Z.L. Wang
School of Materials Science and Engineering, Georgia Institute of Technology, Atlanta, Georgia 30332-0245

Z. Yu, J. Ramdani, R. Droopad, and K.W. Eisenbeiser
Physical Science Research Laboratories, Motorola Inc., Tempe, Arizona 85284

R. Ramesh
Materials Research Science and Engineering Center, University of Maryland, College Park, Maryland 20742

(Received 26 February 2001; accepted 31 October 2001)

Microstructure in the $SrTiO_3$/Si system has been studied using high-resolution transmission electron microscopy and image simulations. $SrTiO_3$ grows heteroepitaxially on Si with the orientation relationship given by $(001)_{STO}//(001)_{Si}$ and $[100]_{STO}//[110]_{Si}$. The lattice misfit between the $SrTiO_3$ thin films and the Si substrate is accommodated by the presence of interfacial dislocations at the Si substrate side. The interface most likely consists of Si bonded to O in $SrTiO_3$. The alternative presentation of Sr and Si atoms along the interface leads to the formation of 2× and 3× Sr configurations. Structural defects in the $SrTiO_3$ thin film mainly consist of tilted domains and dislocations.

I. INTRODUCTION

There is now a considerable effort aimed at the deposition of $SrTiO_3$ (STO) dielectric thin films on silicon substrates since $SrTiO_3$ is an alternative to silica (SiO_2) as the gate dielectric in a field effect transistor.[1–9] SiO_2 has been used as the gate dielectric in a field effect transistor since the 1960's. However, SiO_2-based transistor technology is approaching its fundamental limits: as the SiO_2 thickness scales below 2 nm the gate leakage of the metal oxide semiconductor field effect transistor will become unacceptably high due to excessive tunneling current. Technology road maps for the semiconductor industry predict the need for 2 nm and below gate dielectrics in the near future. A systematic consideration of the required properties of gate dielectric indicates that the key guidelines for selecting an alternative gate dielectric are dielectric constant k, conduction band offset to silicon ΔE_C, interface quality between the gate dielectric and the silicon substrate, film morphology, thermodynamic stability, reliability, etc.[10] Possible alternative gate dielectrics investigated are Ta_2O_5,[11–13] TiO_2,[14] ZrO_2,[15] $ZrSi_xO_x$,[16] $HfSi_xO_x$,[17] and $SrTiO_3$.[1–9] The novel gate oxides must be either epitaxially grown or amorphous to avoid unacceptable scatter of the properties due to granularity effects. Among the reported high-k materials,[1–17] perovskite-type $SrTiO_3$ lends itself as one of the most promising candidates for alternative gate oxide with desirable structural and dielectric properties. Although the reported conduction band offset value for the $SrTiO_3$–Si system is relatively low ($\Delta E_C < 0.5$ eV), which would lead to high leakage current,[10,20] high-quality epitaxy $SrTiO_3$ films grown on silicon substrate are expected to offer better uniformity, lower leakage current, and higher reliability than amorphous and polycrystalline ones.[1,2,8,9]

In STO/Si heterostructures, $SrTiO_3$ has a cubic perovskite-type structure with a lattice parameter of 0.39050 nm and silicon has a diamond structure with a lattice parameter of 0.54088 nm. Due to the dramatic differences in crystal structure and crystal chemistry between the $SrTiO_3$ thin film and the Si substrate, the nature of STO–Si interface and structural defects in the

STO thin film become critical to the structural and chemical integrity of the device and its electrical performance. One of the key problems in growing perovskite films on a silicon substrate is the formation of amorphous SiO_2 at the interface between perovskite oxide and silicon substrate, which ordinarily forms when silicon is exposed to a containing oxygen environment. Fully understanding of the nature of the STO–Si interface and the structural features within the STO thin film at the highest available structural resolution is the primary focus of this work.

The heteroepitaxial growth depends on not only the various interfacial energies but also the film/substrate lattice mismatch as well as on the growth temperature.[21,22] In general, as the mismatch increases, the mode of growth changes from two-dimensional (layer by layer) to three-dimensional (island nucleation and coalescence). The growth mode of two-dimensional followed by island nucleation often takes place at intermediate mismatch values. In an excellent review of epitaxial growth mechanism,[21] the main tendencies in the growth mode are summarized as follows: 3D island formation is favored (1) when the interfacial bonding is weaker than the bonding in the deposit, (2) at higher substrate temperatures, (3) at lower deposition rates, (4) at larger lattice mismatches, and (5) when the film is deposited on less densely-packed substrate surfaces (e.g., $\{100\}_{fcc}$ or $\{100\}_{bcc}$ planes). Conversely, layer by layer growth is favored in systems (1) for which the interfacial bonding is stronger than the bonding in the film material, (2) in which the lattice mismatch is zero (e.g., homoepitaxy) or very small ($\leqslant 0.01\%$), (3) at lower substrate temperature, (4) at higher deposition rates, and (5) when the film is deposited on densely packed substrate surfaces (e.g., $\{111\}_{fcc}$ or $\{110\}_{bcc}$ planes).

Film thickness plays an important role in its microstructural evolution. A major criterion for dislocation formation in thin films is the critical thickness for misfit strain relaxation. If the film is thinner than the critical thickness, lattice strain generated by mismatches accumulates elastically within the film, forming a coherent interface.[23,24] Otherwise, the misfit dislocations are produced rather than elastic accumulation of misfit strain.[23–25] At the critical thickness the formation of misfit dislocations becomes energetically favorable.[26] If the substrate is already dislocated, with some dislocations intersecting its surface, a possible mechanism for the formation of interfacial misfit dislocations is the extension of the substrate dislocations in the film.[27,28] On the other hand, if the substrate is dislocation-free or has a very low density of dislocations, then new dislocations have to nucleate in the film or at the film/substrate interface. In heteroepitaxial systems with small mismatch (including the cases of two-dimensional growth), a likely mechanism is dislocation nucleation at some heterogeneity in the film, usually at the interface.[28] On the other hand, in larger mismatched systems, where film deposition is invariably by (two- or three-dimensional) island growth, dislocation often nucleate at the edges of the island.[29] In this paper, we present our microstructural analysis of STO/Si heterostructures prepared by molecular beam epitaxy (MBE). The investigation of STO–Si interface structures by high-resolution transmission electron microscopy (HRTEM) in conjunction with detailed image simulation reveals some basic and important microstructural characteristics resulted from the effects of lattice, structure, and chemistry misfits.

II. EXPERIMENTS

Commercial Si(001) wafers with size up to 8 in. in diameter were used in the experiment. MBE growth runs were conducted in an upgraded production-type MBE system equipped with a turbo-molecular pump and a titanium-sublimation pump. The growth chamber base pressure is better than 5×10^{-10} mbar. Sr, Ti metals from effusion cells and oxygen were used as deposition sources. *In situ* reflection high-energy electron diffraction was used to monitor the growing surface in real time during growth process. The as-received substrate was transferred into the growth chamber and heated to temperature below 800 °C before exposure to a Sr metal flux, until a (2×1) ordered interface structure was formed on the Si surface. STO films were deposited on such ordered structure at temperature ranging from 300 to 700 °C under up to 10^{-5} mbar O_2 partial pressure in the growth chamber. Specifically, the films used for this study were deposited at a substrate temperature of 700 °C.

To reveal the interface structure between the STO layer and the Si substrate as well as structural defects in STO thin film at atomic level, cross-sectional transmission electron microscopy samples were prepared by following traditional procedures including cutting, gluing, polishing, and ion milling. The samples were cooled to liquid-nitrogen temperature during ion milling to avoid any possible structural damage. HRTEM observations were carried out using a JEOL 4000EX (Tokyo, Japan) microscope with a point to point image resolution of 0.18 nm. The image simulation was performed using the multislice method with MacTmpas program. Relevant instrument parameters include the accelerating voltage, $V = 400$ kV, spherical aberration coefficient, Cs = 1.0 mm, beam divergence, div = 0.55 mrad, and focal spread, Del = 80Å.

III. RESULTS AND DISCUSSION

Cross-sectional transmission electron microscopy has been performed to characterize the STO–Si heterostructures. Figure 1 shows a typical HRTEM image of STO/Si

heterostructures taken with the incident electron beam parallel to the [110] zone axis of the silicon substrate [the corresponding electron diffraction pattern is shown in Fig. 2(a)]. Single-crystal STO thin film with a thickness of 10 nm is epitaxially grown on the (001) surface of silicon substrate. The growth direction is perpendicular to the interface between the STO thin film and the Si substrate. The interface in this case is free of amorphous material. Both top and bottom surfaces of STO are relatively flat and parallel with respect to each other. No interfacial reaction is observed along the STO–Si interface.

Figure 2(a) shows a selected area electron diffraction pattern taken from the common region of the STO thin film and the silicon substrate. The orientation relationship between the STO thin film and the Si substrate in the STO/Si heterostructures is as follows:

$$(001)_{STO}//(001)_{Si} \quad ,$$

$$[100]_{STO}//[110]_{Si} \quad ,$$

i.e., the STO lattice is rotated by 45° around the [001] axis of the silicon lattice on the silicon (001) surface. Since the lattice constants of STO and Si are 0.39050 and 0.54088 nm, respectively, the interplanar distance $d_{(001)}$ of the STO thin film is nearly half of the interplanar distance $d_{(110)}$ of the silicon substrate so that $(001)_{STO}$ fits well on the $(001)_{Si}$ surface if its lattice is rotated by 45° as shown in Fig. 2(b). Here, the lattice misfit parameter, $\delta = 2(d_{(100)STO} - d_{(110)Si})/(d_{(100)STO} + d_{(110)Si})$ between the parallel $(100)_{STO}$ and $(110)_{Si}$ planes that are perpendicular to the interface, is only 1.67%. Since the film was deposited on the (001) plane of silicon (a less densely packed substrate surface) and the lattice mismatch between STO and Si is neither small nor large, the mode of growth is probably of two-dimensional growth followed by island nucleation.[22] The question as to whether Sr, Ti, or O atoms site on the silicon atoms will be discussed in the atomic structure of the interface.

A detailed investigation of the interface structure was carried out along the interface between the STO–Si thin film and the silicon substrate. Figure 3 shows an enlarged HRTEM image of region A in Fig. 1. The STO film epitaxially grew on $(001)_{Si}$ surface, totally avoiding the amorphous silica phase. We observe a tilt of approximately 10° between the $(001)_{STO}$ planes and the $(111)_{Si}$ planes. The arrowheads in opposite directions indicate that atomic columns in STO thin film directly linked with those in the Si substrate through the interface. The dislocation on the silicon substrate side is revealed numbering the atomic columns on both STO and Si sides, respectively. A Burgers circuit around the dislocation

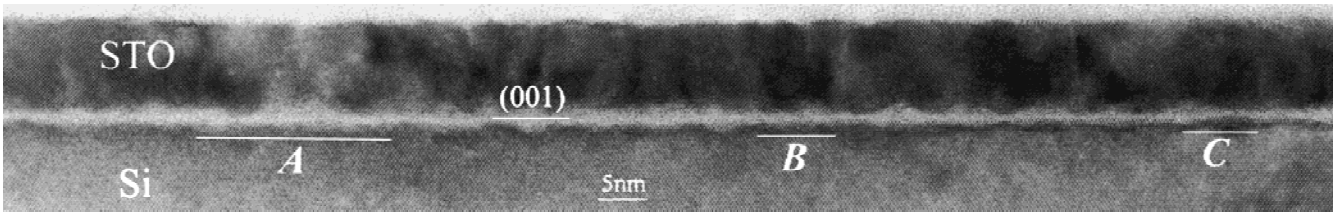

FIG. 1. HRTEM image of the interface between the $SrTiO_3$ thin film and the silicon substrate, showing the epitaxial growth of the single STO thin film on the (001) surface of silicon substrate.

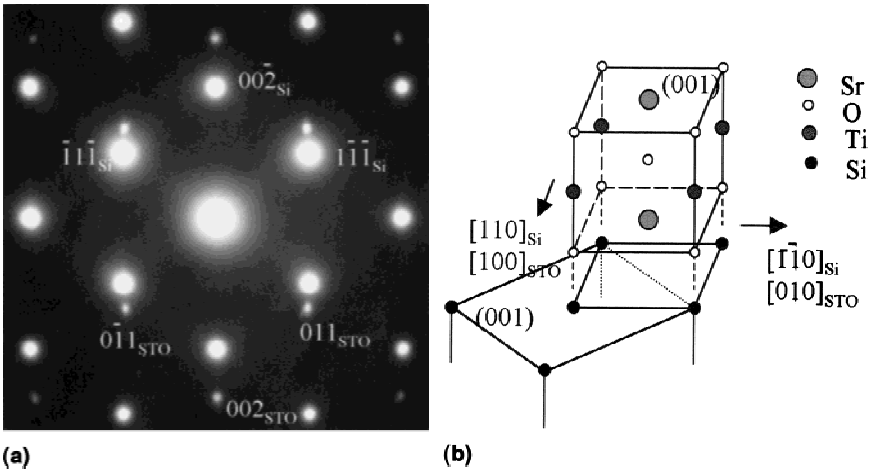

FIG. 2. (a) Selected area electron diffraction pattern taken from an interface region indicating the orientation relationship of $(001)_{STO}//(001)_{Si}$ and $[100]_{STO}//[110]_{Si}$. (b) Schematic presentation of the STO unit cell rotation on the silicon (001) surface.

indicates the Burgers vector is $a/2[1\bar{1}0]$, where a is the lattice constant of the silicon substrate. In general, the density of misfit dislocations at the STO–Si interface is not high since the lattice mismatch between the STO thin film and the silicon substrate is only 1.67% when a unit cell of STO rotated by 45° on a Si(001) surface. The average distance between the two adjacent interface dislocations is theoretically expected to be $L = d_{\{110\}Si}d_{\{100\}STO}/|(d_{\{110\}Si} - d_{\{100\}STO})|$. The calculation of the equation gives $L = 19.34$ nm, which is equal to about $50d_{\{100\}STO}$ or $51d_{\{110\}Si}$. Thus, the interface dislocation is expected on the silicon substrate side, which is in agreement with the experimental observation. The lattice misfit between the substrate and the film is relaxed into local regions of coherent fit separated by the disturbed atomic sequences.

Atomic arrangements at a STO/Si interface have been examined using high-resolution electron microscopy and image simulation. Figure 4 shows an enlarged HRTEM image of region B in Fig. 1. This high-resolution image of the STO/Si interface was recorded at close to optimum defocus so that the atomic columns (also unresolved dumbbell silicon atom columns) appear with black contrast. The basal planes of both the STO thin film and the silicon substrate are horizontal. The specific planes in the vicinity of the interface are shown labeled at 1–5. The plane numbered as "1" shows image contrast of the silicon substrate, and the planes numbered as "3–5" show the image contrast of the $SrTiO_3$ thin film. The plane labeled by "2" serves as a "bridge" from the Si substrate (plane 1) to the STO thin film (plane 3). Since the $SrTiO_3$ crystal has a structure consisting of alternating SrO and TiO_2 atomic planes along the [001] growth direction,[30] either SrO or TiO_2 atomic layer is possible for layers "3–5".

Figure 5(a) shows the interface structure model based on atomic simulation.[31] The left part is a full structure model in which all atoms and bonds are present. The oxygen atoms are modulated at the STO–Si interface layer. The right part shows a simplified model in which only Sr, Ti, and Si atoms are shown. Figure 5(b) shows the results of through-focus and through-thickness image simulations based on the structure model in Fig. 5(a). The simulated images with the interface layers of Sr–O–Si silicate and Sr–Si silicide are respectively shown in the left and right parts. It is evident from the simulated images that the oxygen layer at the interface has little influence on the contrast variation along the interface. The arrowheads in Fig. 5(b) indicate the positions of silicate and silicide configurations in each through-focus series. The image contrast varies only slightly from one to the other with a change of defocus and sample thickness. The simulated image for the foil thickness of 3 nm and a defocus of −35 nm has the characteristics features exhibited in the observed experimental image. The excellent fit to the experimental image indicates that there is a good match between the experimental HRTEM image and the structure model where silicon atoms bonded directly with oxygen atoms on the (001) surface of silicon. Therefore, the atomic layer numbered as "3" is determined as SrO. It is noted that the measured interplanar distances for the atomic layers numbered as 2–3, 3–4, and 4–5, i.e., $d_{\{200\}STO}$, are not identical. The measurements were performed taken the $d_{\{111\}Si}$ as reference in Fig. 4. The interplanar distance between the (200) atomic

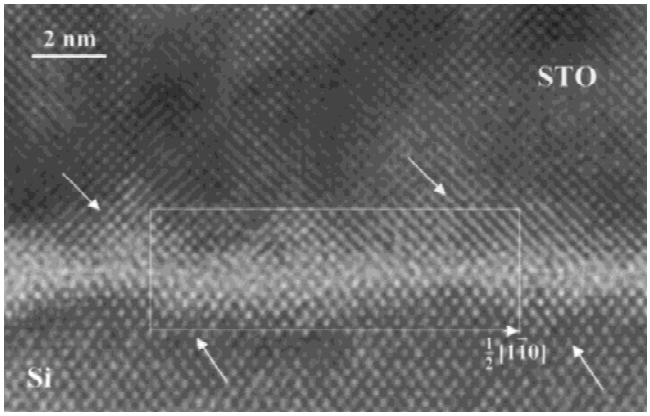

FIG. 3. Enlarged HRTEM image of region A in Fig. 1. Interface dislocation with the Burgers vector of $a/2[110]$ on the Si side accommodates the misfit of lattice constants between the STO thin film and the Si substrate.

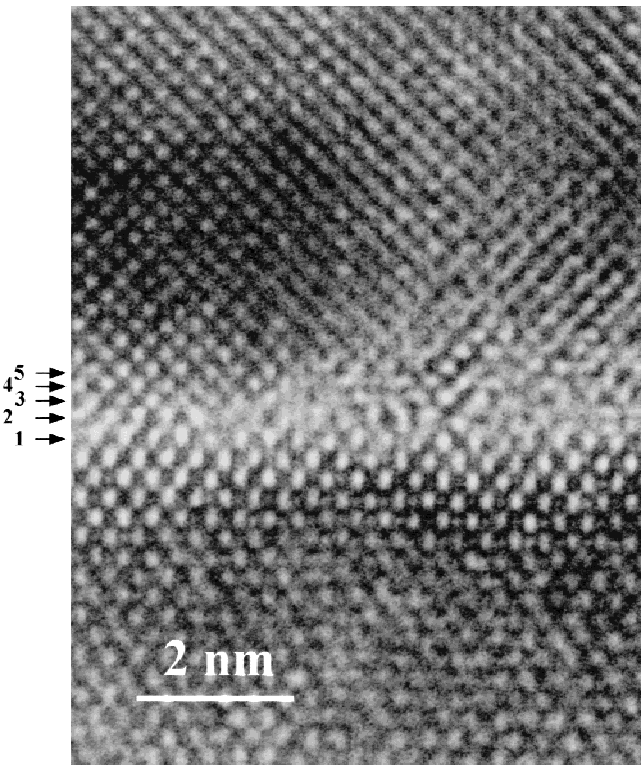

FIG. 4. Enlarged HRTEM image of region B in Fig. 1, showing the sharp interface between the STO thin film and the Si substrate that is noted by the arrowhead numbered as "2".

planes remarked as "2" and "3" ranged from 0.23 to 0.25 nm, but those for "3–4" and "4–5" are approximately identical and they are about 0.2 nm. This suggests that local crystal structure constructed by atomic layers "2" and "3" is probably fcc SrO, which has a lattice parameter of 0.516 nm. Thus, the atomic layers numbered as "4" and "5" are TiO_2 and SrO layers, respectively.

Figure 6 shows a HRTEM image taken from the same cross section of Fig. 4 but from a different region along the interface (region C in Fig. 1). As noted by arrowheads, we observe that the darker and gray dots are alternately present with 2× (darker and gray) and 3× (darker, gray, gray) patterns along the interface. To determine the atomic arrangement at the interface, a 2× structure model is shown in Fig. 7(a).[31] A full structure model is shown in the left part and simplified model is in the right part. Figure 7(b) presents the through-focus and through-thickness image simulations based on the structure model in Fig. 7(a). The simulated images with the interface layers of Sr–O–Si silicate and Sr–Si silicide are respectively shown in the left and right parts. No image contrast variation was found along the interface in the simulated images. Comparison of the atomic model and the simulated images shows that Sr atomic columns appear darker contrast in the simulated images. The simulated image for the foil thickness of 3 nm and a defocus of −35 nm shows an excellent fit to the experimental image, indicating that there is a good match between the experimental HRTEM image and the structure model.

We note that, in Fig. 6, the darker contrast of Sr atomic columns varies slightly along the STO–Si interface. To explain this variation, we speculate that there is the possibility of local structural fluctuations in the interface structure. We assumed three types of configurations are present between these domains as illustrated schematically in Fig. 8. The solid lines in the schematics in Fig. 8 show these Sr atomic column configurations, where "t" represents the sample thickness along the observation direction. The straight Sr atomic column runs along the incident beam direction in the first model [Fig. 8(a)]; the Sr atomic column is almost straight, but it runs obliquely to the incident beam direction in the second model. In the third model, the Sr atomic column has a zigzag shape. It is reasonable to suggest that a straight Sr atomic column parallel to the incident beam direction

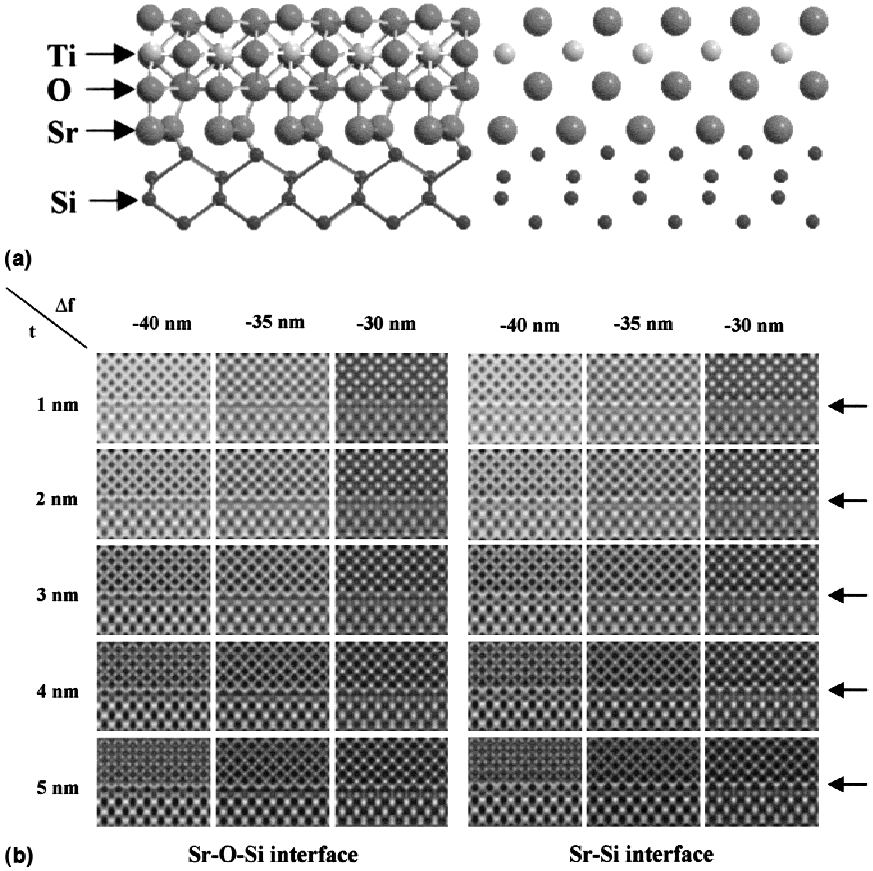

FIG. 5. (a) 1× interface structure model based on atomic simulation. (b) Through-focus and through-thickness image simulations. The image contrast is consistent in the left part formed with Sr–O–Si silicate interface and in the right part with Sr–Si silicide interface, respectively.

gives a sharp and darker image while a Sr atomic column running obliquely to the incident beam direction or a zigzag leads to an intensity changes along the interface.

Figures 4 and 6 describe the structure transition from silicon to $SrTiO_3$ ionic oxide. It was established that the $SrTiO_3$/Si interface was abrupt to within one atomic plane and the interface most likely consists of Si bonded with O in $SrTiO_3$. The alternative presentation of Sr and Si atoms along the interface leads to the formation of 2× and 3× Sr configurations. The study of crystalline oxides on silicon by Z contrast image[2] showed the presence of oxide-free 2 × 1 and 4 × 2 silicide layers. However, atomic simulation results[31] indicate a layer consisting of Sr, Si, and O forming a 2 × 1 periodicity at the STO/Si interface is energetically favorable. The 1× and 2× periodicity can be observed from two orthogonal directions, namely [011] and [01$\bar{1}$]. The additional 3× periodicity reported in this paper indicates that the interface is more complex than what was published before.[2,31] It suggests that Sr at the interface forms alternating domains of 2 × 1 and 3 × 1 shown in Figs. 4 and 6. The observed difference of the interface structure could be related to the method used in forming the STO/Si interface in this study. Due to the limitation of the techniques used, the presence of the oxygen at the interface between the STO thin film and Si substrate could not be identified unambiguously by HRTEM. While the structure of the interface needs further discussion, some conclusions may be drawn on the arrangement of Sr and Si at the interface. It is clearly shown by all studies that Sr is closely packed in one direction than the other at the interface of STO/Si and there are Si atoms separating Sr atoms in the direction where Sr are loosely packed. The presence of oxygen in the interface layer is likely to be the case from the considerations of the growth process and the simulation results.

An important structural feature in the STO/Si heterostructure is its high density of structure defects in STO thin film. It is known that the structure and lattice match at the interface are critically important for thin-film growth, because many defects in the film are directly nucleated at the interface defects, such as steps on the surface substrate. Figure 9(a) shows a cross-sectional HRTEM image of a STO/Si heterostructure taken with the incident electron beam parallel to the [110] zone axis of silicon substrate. Numerous structural defects have been observed in STO thin film although no structural imperfection is present within the Si substrate. The STO film shows distinctive contrast in the regions marked as A, B, C, and D, and the intensities of atomic columns in each region are fairly uniform. The variation of image contrast is an indication of slight misorientation between adjacent domains although this misorientation may not be successfully revealed by electron diffraction along the direction parallel to the interface. The domain tilt is confined in the (010) or the (100) plane, a plane perpendicular to the STO–Si interface. The interface between STO and Si is quite rough, containing a number of atomic steps along the interface. Each step can be considered as an interface dislocation with its Burgers vector perpendicular to the interface. It has been found that most of the misorientation is directly related with the surface steps, as indicated by paired arrowheads in the image. The step height (or facet height) on the Si substrate ranges from 1 to 3 atomic layers along [001] growth direction of STO thin film. The orientation variation of STO thin film originates at the $(001)_{Si}$ surface, where an atomic step is present, and ends at the top of the film. The creation of misorientation between adjacent regions across a substrate step is very natural during lattice reorientation because the film is grown in the mode of layer by layer from the surface of the substrate; thus, the first layer is grown by following the topography of the substrate. Taking $(100)_{STO}$ or $(010)_{STO}$ planes as the slip planes, the lattice rotation within $(100)_{STO}$ or $(010)_{STO}$ is expected as misfit segments at the interface due to the presence of interfacial dislocation with its Burgers vector perpendicular to the interface. The domains A, B, C, and D were formed by a 3D island growth. Therefore, the presence of a step and its height is directly related to the

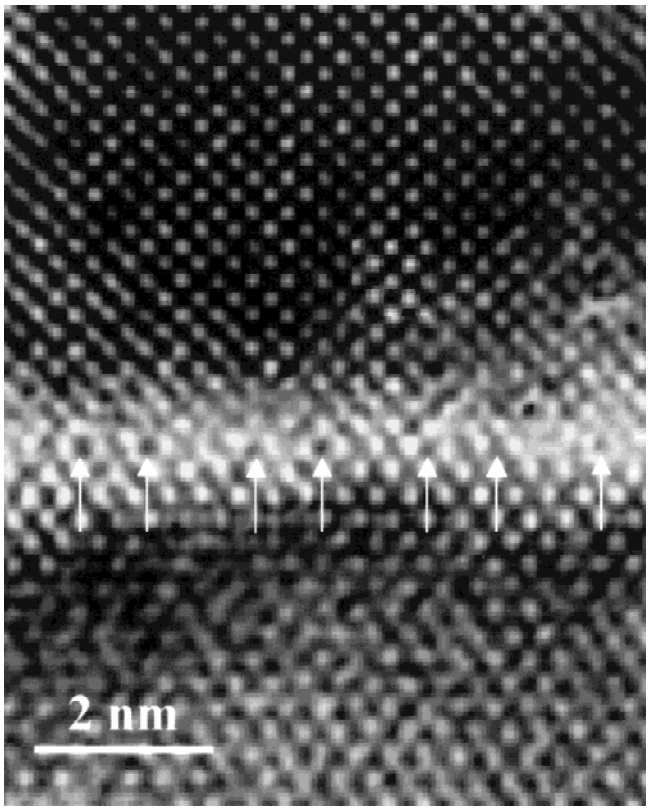

FIG. 6. Enlarged HRTEM image of region C in Fig. 1, showing 2× and 3× darker and gray dots along the interface.

misorientation between different domains within the STO film on the basis of the fact that the interplanar distance $d_{(001)STO}$ differs from $d_{(001)Si}$ as well as the lattice reorientation took place during the deposition of STO film on the Si(001) surface.

In addition to the above domain tilt, structural defects are also frequently observed, which are confined within 5 nm from the interface between the STO thin film and the silicon substrate. The density of such defects can be quite high in some local regions, as marked by the white arrowheads in Fig. 9(a). To reveal clearly the detail of the structural defects, an enlarged image is shown in Fig. 9(b). The fine lines indicate the atomic columns in STO thin film. As noted by the white arrowheads, the dislocations are revealed through numbering the atomic columns between the fine line pairs. The Burgers circuits around the dislocations indicate the Burgers vectors of $a/2[011]$ and $a/2[011]$, where a is the lattice constant of STO. As marked by the symbols "T" and "inverted T" in the left part of the image, there are a few dislocations in STO thin film that come in pairs with opposite characters, i.e., each pair forms a dipole. The total Burgers vector around the dislocation pair is zero, and they make no contribution to the lattice accommodation. It is obvious that the simultaneous presence of two dislocations with opposite sign could effectively minimize the strain resulting from the creation of one dislocation. Compared with domain (A, B, C, and D) tilt running through STO thin film, dislocations are confined within the film. This implies that the dislocations were also probably introduced in the STO crystal growth process; i.e., both the Si substrate surface roughness and single STO thin film growth process could affect the structural perfection of the STO thin film.

To fully understand the structural defects in the STO thin film, a TEM observation of a plan-view specimen with the incident beam perpendicular to the substrate surface was carried out. Figure 10 shows some important structure features observed along the direction perpendicular to STO–Si interface. Figure 10(a) is a plan-view TEM micrograph of STO thin film taken with the incidence parallel to the [011] zone axis of STO that is perpendicular to the STO–Si interface. The corresponding selected area electron diffraction pattern is shown in Fig. 10(b). Most of the defects lie in the (100), (111), or (1$\bar{1}$1) planes. In the electron diffraction pattern in

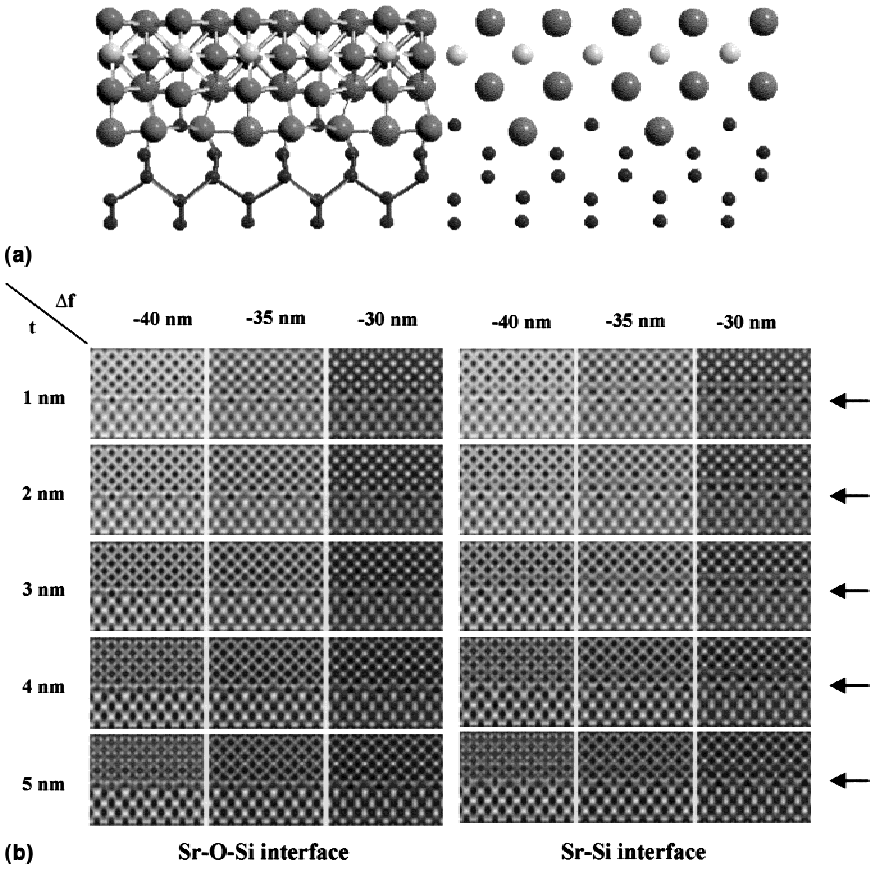

FIG. 7. (a) 2× interface structure model based on atomic simulation and (b) simulated HRTEM images pattern with changing defocus and sample thickness. The darker dots and gray dots correspond to the strontium atomic columns and the silicon atomic columns, respectively. The image contrast is consistent in the left part formed with Sr–O–Si silicate interface and in the right part with Sr–Si silicide interface.

Fig. 10(b), the enlarged reflection around the transmitted spot is an indication of <3° tilt between different domains in STO film.

The observation at atomic level of domain structure in STO thin film was performed by HRTEM with a plan-view TEM sample. Figure 11(a) shows an experimental HRTEM image of STO film taken along the $[011]_{STO}$ direction. As denoted by paired arrowheads in the image, the curved (100) plane is observed between A and B due to domain tilt in the [011] direction. A similar structural feature is also present for A and D domains. Specifically, a stacking fault of displacement vector $R = \frac{1}{2}[100]$ is seen between B and C domains. A careful analysis of the image contrast in this region suggests that the B–C domain interface is inclined with respect to the incident electron beam direction, as illustrated schematically in Fig. 11(b). The displacement of B domain with respect to C domain along the [100] direction results in a $\frac{1}{2}d_{(100)}$ lattice displacement. Therefore, in the HR-TEM image, adjacent domains translating and overlapping should be responsible for the presence of the fine image contrast.

IV. CONCLUSIONS

The investigation of microstructural characteristics in STO/Si heterostructures prepared by MBE was performed using high-resolution transmission electron microscopy (HRTEM) and image simulations. The results can be grouped as follows:

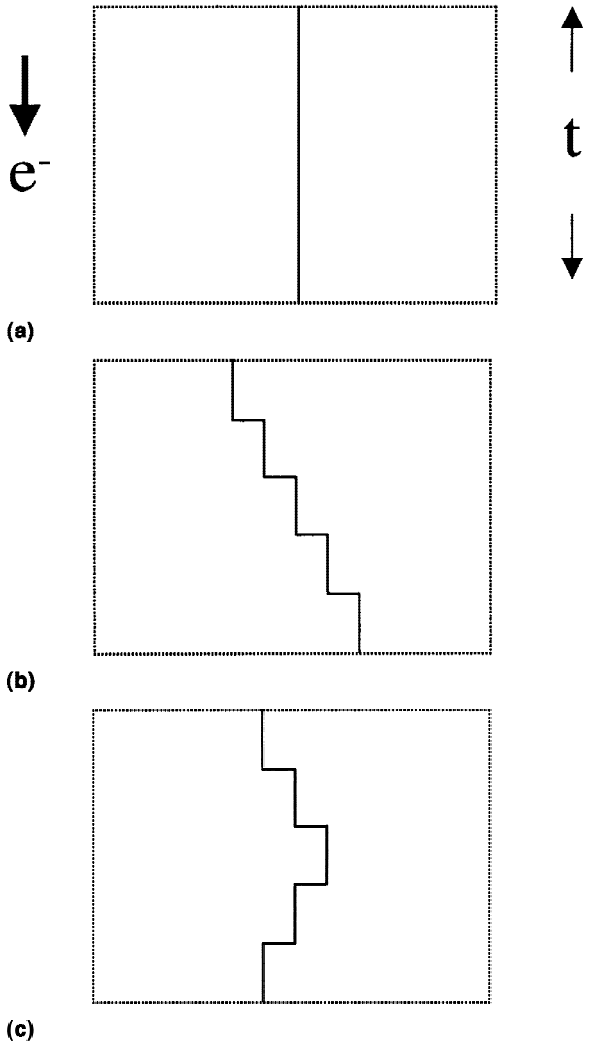

FIG. 8. Three possible configurations of Sr atomic column along the incident electron beam direction: (a) straight Sr atomic column; (b) oblique Sr atomic column; (c) Sr atomic column having a zigzag shape.

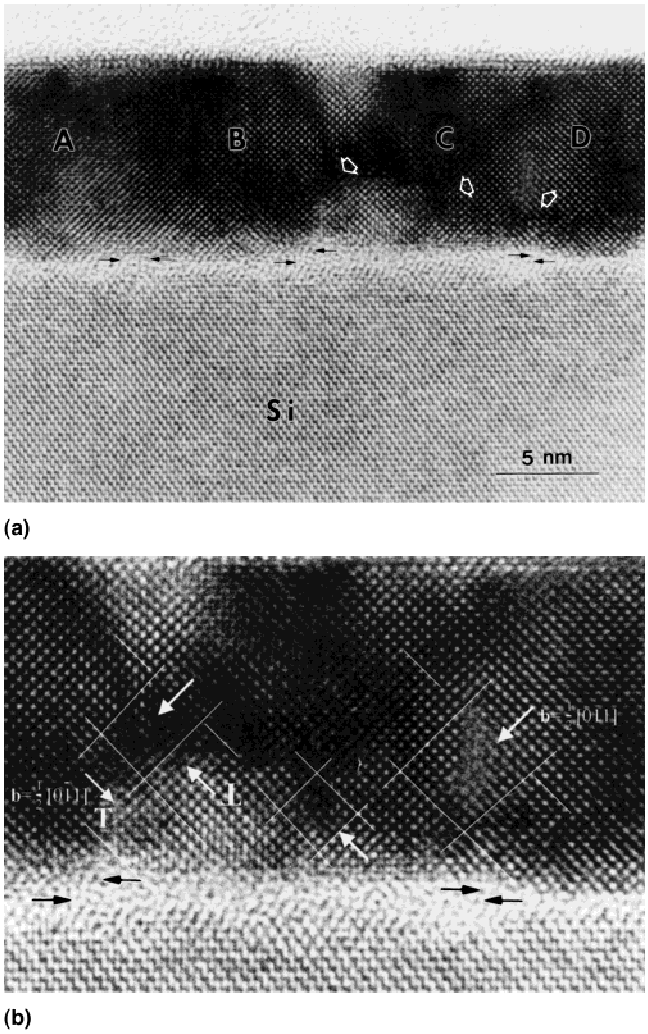

FIG. 9. Cross-sectional HRTEM image of the STO–Si interface taken with the incidence being parallel to $[100]_{STO}//[110]_{Si}$, showing the presence of structural defects in STO thin film. Correlation between misorientation of different regions in STO thin film and the substrate steps is indicated by the paired arrowheads in (a), and dislocations with the vectors of $\frac{1}{2}[011]$ and $\frac{1}{2}[011]$ are clearly shown in (b).

(1) Single-crystalline $SrTiO_3$ (STO) thin film with a thickness of 10 nm has been epitaxially grown on the single crystalline Si(001) surface. Along an STO–Si interface free of amorphous phases, the interface is atomically sharp and no interfacial reaction layer is observed.

(2) The orientation relationship between the STO thin film and Si can be described as $(001)_{STO}//(001)_{Si}$ and $[100]_{STO}//[110]_{Si}$. STO lattice rotation on Si(001) surface is expected to efficiently minimize the dramatic difference in crystallographic parameters and crystal chemistry between the $SrTiO_3$ thin film and the silicon substrate.

(3) A detailed study of interface structure shows that the lattice mismatch of only 1.67% at STO–Si interface could be accommodated by the presence of interface dislocations on the Si substrate side.

(4) The STO–Si interface is abrupt to within one atomic plane and the termination from the STO side is SrO layer. It is connected to the silicon substrate through an interfacial layer that consists of Sr, Si, and most likely O.

(5) Arrangement of Sr atoms in the interfacial layer is anisotropic. They are closely packed in one area than in the others. There are Si atoms separating Sr atoms in the loosely packed areas, and they appear to have 2× or 3× periodicity.

(6) Structural defects in the STO thin film mainly consist of tilted domains (misorientation) and dislocations. Atomic steps on the Si(001) surface induced the misorientation between adjacent regions in STO film. The dislocations confined within 5 nm from the interface may be resulted from the silicon (001) roughness and layer by layer deposition.

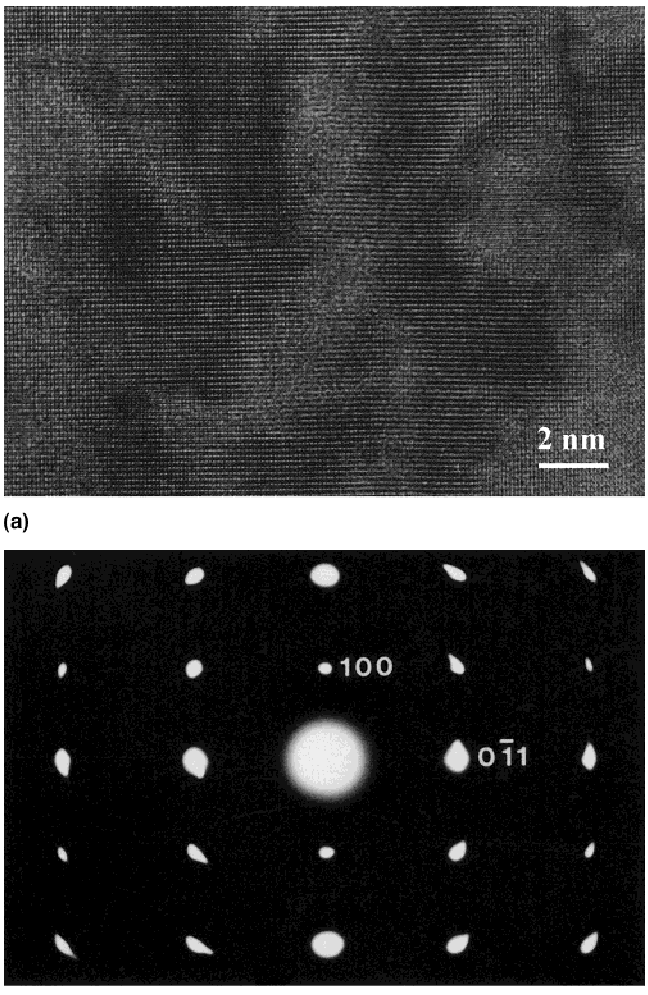

FIG. 10. (a) Plan-view TEM image revealing the domain structure of STO thin film and (b), corresponding selected area electron diffraction pattern. The curved spot indicating the domain tilt among different domains in the STO thin film.

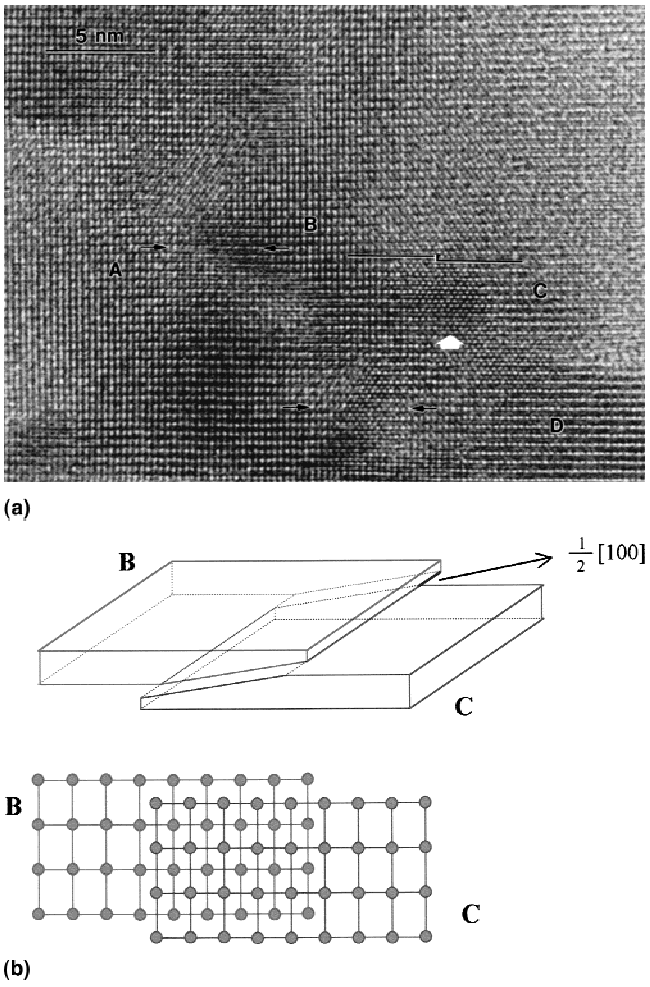

FIG. 11. (a) HRTEM image of STO thin film taken along the direction perpendicular to STO top surface, showing the domain tilt resulted from curved (100) plane and stacking fault of displacement vector $R = ½[100]$. (b) Schematic drawing of domain displacement and overlapping with respect to each other.

ACKNOWLEDGMENT

This work is supported by a National Science Foundation Materials Research Science and Engineering Center (MRSEC) under Grant No. DMR-00-80008.

REFERENCES

1. K. Eisenbeiser, J.M. Finder, Z. Yu, J. Ramdani, J.A. Curless, J.A. Hallmark, R.W. Droopad, J. Ooms, L. Salem, S. Bradshaw, and C.D. Overgaard, Appl. Phys. Lett. **76,** 1324 (2000).
2. R.A. McKee, F.J. Walker, and M.F. Chisholm, Phys. Rev. Lett. **81,** 3014 (1998).
3. H. Mori and H. Ishiwara, Jpn. J. Appl. Phys., Part 2 **30,** L1415 (1991).
4. Z. Yu, R. Droopad, J. Ramdani, J.A. Curless, C.D. Overgaard, J.M. Finder, K. Eisenbeiser, J. Wang, J.A. Hallmark, and W.J. Ooms, in *Ultrathin SiO_2 and High-K Materials for ULSI Gate Dielectrics*, edited by H.R. Hubb, C.A. Richter, M.L. Green, G. Lucovsky, and T. Hattori (Mater. Res. Soc. Symp. Proc. **567,** Warrendale, PA, 1999), p. 427.
5. B. Moon and H. Ishiwara, Jpn. J. Appl. Phys., Part 1 **33,** 1472 (1994).
6. R.A. McKee, F.J. Walker, and M.F. Chisholm, in *Ultrathin SiO_2 and High-K Materials for ULSI Gate Dielectrics*, edited by H.R. Hubb, C.A. RIchter, M.L. Green, G. Lucovsky, and T. Hattori (Mater. Res. Soc. Symp. Proc. **567,** Warrendale, PA, 1999), p. 415.
7. N. Setter and R. Waser, Acta Mater. **48,** 151 (2000).
8. Z. Yu, J. Ramdani, J.A. Curless, J.M. Finder, C.D. Overgaard, R. Droopad, K.W. Eisenbeiser, J.A. Hallmark, and W.J. Ooms, J. Vac. Sci. Technol. B **18,** 1653 (2000).
9. Z. Yu, J. Ramdani, J.A. Curless, C.D. Overgaard, J.M. Finder, R. Droopad, K.W. Eisenbeiser, J.A. Hallmark, and W.J. Ooms, J. Vac. Sci. Technol. B **18,** 2139 (2000).
10. G.D. Wilk, R.M. Wallace, and J.M. Anthony, J. Appl. Phys. **89,** 5243 (2001).
11. I. Kizilyalli, R. Huang, and P. Roy, IEEE Electron Device Lett. **19,** 423 (1998).
12. D. Park, Y.C. King, Q. Lu, T.J. King, C. Hu, A. Kalnitsky, S.P. Tay, and C. Cheng, IEEE Electron Device Lett. **19,** 441 (1998).
13. P.K. Roy and I.C. Kizilyalli, Appl. Phys. Lett. **72,** 2835 (1998).
14. K. Yokota, T. Yamada, F. Miyashita, K. Hirai, H. Takano, and M. Kumagai, Thin Solid Films **344,** 109 (1998).
15. M. Morita, H. Fukumoto, T. Imura, and Y. Osaka, J. Appl. Phys. **58,** 2407 (1985).
16. G.D. Wilk and R.M. Wallace, Appl. Phys. Lett. **76,** 112 (2000).
17. G.D. Wilk and R.M. Wallace, Appl. Phys. Lett. **74,** 2854 (1999).
18. I. Markov and S. Stoyanov, Contemp. Phys. **28,** 267 (1987).
19. Y. Ikuhara and P. Pirouz, Microsc. Res. Tech. **40,** 206 (1998).
20. J. Robertson, J. Vac. Sci. Technol. B **18,** 1785 (2000).
21. J.H. Van der Merwe, Philos. Mag. **7,** 1433 (1962).
22. J.H. Van der Merwe, J. Appl. Phys. **34,** 117 (1963).
23. J.W. Matthews, J. Vac. Sci. Technol. **12,** 126 (1975).
24. J.W. Matthews and A.E. Blakeslee, J. Crys. Growth **27,** 118 (1974).
25. J.W. Matthews and A.E. Blakeslee, J. Crys. Growth **32,** 265 (1976).
26. J.P. Hirth, Acta Mater. **48,** 93 (2000).
27. J.W. Matthews, Philos. Mag. **13,** 1207 (1966).
28. J.W. Matthews, S. Mader, and T.B. Light, J. Appl. Phys. **41,** 3800 (1970).
29. R. Vincent, Philos. Mag. **19,** 1127 (1969).
30. M. Kawasaki, K. Takahashi, T. Maeda, R. Tsuchiya, M. Shinohara, O. Ishiyama, T. Yonezawa, M. Yoshimoto, and H. Koinuma, Science **266,** 1540 (1994).
31. J. Wang, J. Hallmark, D.S. Marshall, W.J. Ooms, P. Ordejon, J. Junquera, X. Hu, X. Yao, and D. Sarid, presented at the APS Centennial Meeting, Atlanta, GA, March 20–26, 1999. And personal exchange of results with Dr. Jun Wang.